Monolayered versus multilayered electroless NiP coatings: Impact of the plating approach on the microstructure, mechanical and corrosion properties

Monolayered versus multilayered electroless NiP coatings: Impact of the plating approach on the microstructure, mechanical and corrosion properties of the coatings

A. Salicio-Paz, H. Grande, E. Pellicer, J. Sort, J. Fornell, R. Offoiach, M. Lekka, E. García-Lecina

PII: S0257-8972(19)30378-0
DOI: https://doi.org/10.1016/j.surfcoat.2019.04.013
Reference: SCT 24508

To appear in: *Surface & Coatings Technology*

Received date: 15 December 2018
Revised date: 8 March 2019
Accepted date: 3 April 2019

Please cite this article as: A. Salicio-Paz, H. Grande, E. Pellicer, et al., Monolayered versus multilayered electroless NiP coatings: Impact of the plating approach on the microstructure, mechanical and corrosion properties of the coatings, Surface & Coatings Technology, https://doi.org/10.1016/j.surfcoat.2019.04.013

Monolayered versus multilayered electroless NiP coatings: impact of the plating approach on the microstructure, mechanical and corrosion properties of the coatings

A. Salicio-Paz[1], H. Grande[1], E. Pellicer[2], J. Sort[2,3], J. Fornell[2], R. Offoiach[4], M. Lekka[4], E. García-Lecina[1,*]

[1]CIDETEC, Paseo Miramón 196, 20014 Donostia- San Sebastián, Spain

[2]Departament de Física, Universitat Autònoma de Barcelona, E-08193 Bellaterra, Spain

[3]Institució Catalana de Recerca i Estudis Avançats (ICREA), Pg. Lluís Companys 23, E-08180 Barcelona, Spain

[4]Polytechnic Department of Engineering and Architecture, University of Udine, Udine, Italy

*Corresponding author. *E*-mail address: egarcia@cidetec.es

Abstract

Electroless nickel-phosphorous (NiP) coatings were produced on low carbon steel substrates for a total plating time of 3 h. Different preparation modalities were pursued. Multilayered coatings were produced by stacking three layers of the same composition by successive electroless plating with rinsing steps in between. On the other hand, coatings termed ‘monolayered’ for the sake of comparison were deposited by one step electroless process, with and without undergoing bath replenishment of the electrolyte during plating. All the samples were subjected to thermal annealing at 400 ºC for 1 h under argon atmosphere.

The results show that the multilayer approach prevents crack propagation in the as-deposited coatings because the interfaces between layers block the advance of defects. Bath replenishment during monolayered coatings production creates pseudo-interfaces similar to those of the multilayered case but they are ineffective in terms of corrosion protection. Un-replenishment of the electrolyte promotes a change in the coating's microstructure from lamellar to columnar which severely worsens their performance. Upon annealing, the presence of interfaces, along with the recrystallization of the metallic matrix, promotes an upgrading of the corrosion performance of the multi-layered coatings. The corrosion products spread laterally at the interface where they stockpile. At a certain point, the accumulation of these by-products provokes the exfoliation of the outermost layer exposing the layer underneath to the corrosive media, thereby delaying the advancement of the corrosion attack. The results of this study highlight the importance of the plating approach selection, as well as the need for proper electrolyte maintenance during the production of high-performance electroless coatings.

Keywords

Electroless nickel plating; Multilayers; Corrosion resistance; Interface; Annealing

1. Introduction

Electroless nickel plating was firstly reported in the seminal paper by Brenner and Riddell, published in 1946 [1]. Since then, and based on their excellent mechanical properties and corrosion resistance, it has become one of the preferred engineering solutions for high demanding applications [2]. Recently, the increasingly stringent environmental regulations on the use of hexavalent chromium has pushed, both in academia and plating industries, the need for more sustainable alternatives to hexavalent chromium [3,4]. Hexavalent hard chromium deposits stand out for their excellent mechanical properties, including hardness and wear, as well as their superior corrosion resistance in functional applications [5]. Electroless nickel coatings have emerged over the last few years as a realistic alternative to hexavalent chromium [6].

In electroless processes, the electrons required to reduce the metallic cations (e.g. Ni^{2+}) are provided by a reducing agent, present in the electrolyte, without the assistance of electrical current [7]. The resulting deposit is an alloy because the reducing agent gets incorporated into the growing layer (e.g., P), thereby enhancing the properties of the bare metal (e.g. Ni) [8]. Among all the metals that can be electrolessly plated, nickel and its alloys represent 95% of all the industrial applications, ~~being~~ hypophosphite being the most used reducing agent [9]. The properties of nickel-phosphorous (NiP) coatings greatly depend on the phosphorous content in the alloy. Accordingly, three main classes of NiP coatings exist. Low phosphorous coatings (1-5 wt.% P) exhibit very good mechanical properties at the expense of limited corrosion resistance. High phosphorous coatings (10-14 wt.% P) present superior corrosion resistance but poor mechanical properties. Medium P content coatings (6-9 wt.% P) offer a good compromise over the formers in terms of mechanical properties and corrosion resistance [10].

This versatility in terms of composition derived properties has broadened the application fields of electroless nickel, which is indeed the preferred solution in the automotive industry, electronics, petrochemical and aeronautics sectors [2,11–14]. These application fields match those in which hard chromium coatings were historically employed for the enhancement of properties of base materials commonly employed in engineering applications. Additionally, the performance offered for as-deposited electroless NiP coatings can be further enhanced by subjecting the coatings to thermal annealing. Generally, annealing at 400 ºC during 1 h under inert atmosphere offers the maximum increase in the properties due to nickel matrix re-crystallization and Ni_3P phase precipitation [15]. Meanwhile, crack development during hard chromium plating has a detrimental effect on their corrosion resistance, which is even magnified upon annealing [16]. This underpins the role of electroless nickel as an alternative to hexavalent chromium plating.

In traditional one-step electrodeposition, the properties of the NiP coatings are dictated by the P content, excluding the possibility to bring together the properties of NiP layers with dissimilar P content in the same structure [17]. In recent years, especially in the plating industry, multilayered coatings have gained much attention due to the advantages offered by these coatings in terms of mechanical and electrochemical behaviour [18]. Narayanan et al. reported the production of electroless multilayered coatings and showed that their corrosion resistance improved if properly selecting the outer layer [17]. Similar results were found by Gu et al. in multilayered systems by incorporating an intermediate electrolytic nickel layer [19]. Recently, Vitry et al. showed the beneficial effect of combining NiP and NiB monolayers in the same deposit. The resulting coatings showed superior wear resistance while maintaining a good corrosion resistance when compared to single layered coatings [20]. As can be inferred from the above, the combination of different layers into a coating offers the possibility to enhance the performance, and thus broaden the functionalities, over single

layered materials. Despite the progress in the field, little attention has been paid to the effect of the interfaces present in multilayered systems.

Therefore, the purpose of this investigation is to deepen into the understanding of the impact of the multilayer plating approach, particularly on the role of the interfaces, on the properties of electroless NiP coatings. For the study, an optimised electroless low phosphorus formulation, combining the best performance in terms of corrosion resistance while maintaining its excellent mechanical properties, has been employed (unpublished results). The low phosphorous electroless nickel layers were sequentially stacked to give rise to the multilayered coating. Their mechanical and corrosion resistance properties were compared to those of monolayered deposits of the same thickness grown by one step electroless deposition. The effect of bath replenishment during electroless nickel plating of the monolayers was also investigated. The impact of the plating approach on the microstructure of the coatings as well as on their mechanical properties and corrosion resistance is assessed.

2. Materials and methods

2.1. Electroless nickel bath and plating approach

A proprietary low phosphorous electroless nickel electrolyte was employed in this investigation. The volume of the electrolyte was 1 litre in all the cases. The nickel concentration in the electrolyte was 6.5 g L^{-1} and sodium hypophosphite was used as reducing agent at a concentration of 20 g L^{-1}. Nature and concentration range of complexing agents, buffers and stabiliser present in the electrolyte remain undisclosed due to confidentiality issues. It is worth mentioning that the electrolyte was organically stabilised, thus avoiding the use of heavy metals as stabilisers to meet the criteria established in the RoHS and ELV directives [21]. The pH of the solution was maintained at 6.5 by NH_4OH or 10% H_2SO_4 correction. The working temperature was set at 75 ºC by means of a PT-1000 probe attached to the magnetic stirrer at ω = 250 rpm (IKA, RTC Basic). All the chemicals used in the

preparation of electroless baths were of analytical grade and dissolved in deionized (DI) water. The total plating time was 3 h for all coatings.

Three different plating conditions were considered in this work. The multilayer approach involved removing the sample from the electrolyte following the first electroless cycle (1 hour), rinsing it in DI water and immersing the coating in H_2SO_4 10% solution to avoid surface oxidation before the second and third electroless steps were attempted. In the interim, the exhausted components of the electrolyte were replenished, and the pH readjusted to its initial value. Electrolyte´s replenishment consisted in Ni^{2+} and $H_2PO_2^-$ addition to the electrolyte from freshly prepared stock solutions. Complexing agents, stabilisers and buffers were also added accordingly. Higher stirring rate was used during replenishment events to assure proper solution homogenization. On the other hand, electroless plating was done only once and the resulting coatings are generically labelled as 'monolayer' for the sake of comparison with the trilayered coatings fabricated on purpose. Chemistry replenishment of the electrolyte while plating was performed hourly in some cases without withdrawing the coating from the electrolyte. The resulting coatings are termed 'rebalanced monolayer (r-monolayer).' Alternatively, one step plating was also performed without readjustment of the chemistry of the solution; this type of coatings is named 'un-rebalanced monolayer (ur-monolayer)'.

In order to study the effect of the thermal treatment on the properties of the coatings, all the samples were subjected to a thermal annealing process. A tubular furnace (Hobersal, ST1611580) was employed for the annealing of the samples at 400 ºC for 1 h time at a heating rate of 10^{o} min^{-1}.The process was carried out under argon atmosphere in order to prevent from surface oxidation. The system was properly purged with argon three times before starting the heating routine to assure the protective environment inside the SiC tube. Once the annealing process was completed, the samples were kept inside so allowing natural cooling to room temperature.

2.2. Substrate preparation

Low carbon steel (AISI-1010) flat foils (75 x 100x 0.6 mm^3) were used as working electrodes. The surface/volume ratio was fixed to 1.5 dm^2 L^{-1} for all studied conditions. Prior to plating, the substrates were chemically degreased and rinsed thoroughly afterwards. Then, electrolytic degreasing was carried out with a cathodic/anodic cycle for 2 and 1 min, respectively. After rinsing, the samples were etched in an HCl 40%: H_2SO_4 5% (v/v) mixture for 3 min before electroless nickel plating.

2.3. Characterization

Surface topography and cross-section morphology of the specimens were examined by field-emission scanning electron microscopy (FESEM) (CARL ZEISS ULTRA PLUS). The weight percentage of phosphorous incorporated into the deposit was determined using an energy dispersive X-ray (Ametek® EDAX, APOLLO X EDX) detector coupled to the electron microscope. For cross-section analysis, representative coated areas of the substrate were cut and embedded in hot mounting epoxy resin. Samples were polished with SiC paper (120-4000 grit) and diamond paste down to 1 µm to achieve a mirror-like finishing of the embedded sample. Chemical etching was carried out in all samples using an HNO_3:CH_3COOH (1/1) mixture for microstructural observation.

Composition of the coatings was analysed by means of glow discharge optical emission spectroscopy (GDOES) using a JY RF-GD PROFILER HR instrument (Horiba Jobin-Yvon). During GDOES experiments the samples were sputtered at an Ar pressure of 650 Pa under an applied power of 35 W. Confocal microscopy (Leica Microsystems, DCM 3D) was used to evaluate surface roughness of the as-deposited coatings as well as surface topography of both as-deposited and annealed coatings. A blue light source (λ= 470 nm) was employed for better resolution with objective magnification of 20 x and 50 x for high resolution images. The obtained images were analysed with the LeicaMap software (Leica

Microsystems). The microstructure was investigated by means of X-ray diffraction (Bruker, D8) using CuK_{α} radiation in the Bragg Brentano geometry. Crystallite size was evaluated using the Scherrer's equation which is implemented in the EVA software® (Bruker) of the diffractometer.

The hardness and reduced Young's modulus of the obtained coatings were evaluated using a nanoindenter (Anton-Paar, NHT^2 model) equipped with a Berkovich pyramidal-shaped diamond tip operating under load control mode. To determine the variation of hardness along the coatings' thickness, 45 indentations were made on their cross-sections, distributed into three separate rows parallel to the substrate surface (i.e., in a region close to the substrate, in the middle, and in a region close to the air surface of the coating). L1 (line 1), L2 (line 2) and L3 (line 3) were located at ~3.5, ~11 and ~17 μm from the substrate, respectively. The maximum applied load was 10 mN with a holding time of 10 s, and a loading/unloading rate of 20 mN min^{-1}. Prior to nanoindentation, cross-sections of the samples were embedded in hot resin and were mechanically polished with 1μm diamond suspension as the last step.

The corrosion resistance of the coatings was evaluated by electrochemical techniques by means of a potentiostat/galvanostat (Biologic, VMP3). All measurements were conducted in an aerated 3.5 wt.% NaCl solution at room temperature in a typical three electrode cell configuration (flat cell; EG&G Princeton Applied Research, Oak Ridge, TN, USA) and with a geometrical working area of 1 cm^2. A Pt mesh and Ag/AgCl/NaCl (3 M) electrode were used as counter and reference electrodes, respectively. At immersion, the samples´ corrosion potential, E_{corr}, was measured and recorded until no further changes were observed (less than 10 mV h^{-1}). In order to obtain the anodic and cathodic Tafel slopes (b_a, b_c), partial potentiodynamic scans (0.1667 mV s^{-1}) on different areas of the same sample were performed, starting from the open circuit potential in the anodic or cathodic direction. The corrosion current density (j_{corr}) was calculated by means of Stern-Geary relation[22].

3. Results and discussion

3.1. Morphology and composition of obtained coatings

After the plating process, the surface of all the NiP coatings presented a lustrous silvery-white appearance for the unaided eye. Surface evaluation by FESEM showed that all samples present the typical globular ~~structure~~ topography of electroless coatings before (Figure 1 a-c) and after annealing (Figure 2 a-c). In all cases they were dense, homogeneous and relatively smooth as can be inferred from the average surface roughness (S_a) values listed in Table 1. The smoothness is maintained after annealing. However, a close-up look of the surface topography showed that the multilayered and r-monolayered exhibit a very similar defect-free surface morphology, whereas small pores and/or defects can be clearly observed on the surface of the ur-monoloyered ones. A priori, one would expect to find more defects on the ur-monolayered coating produced without electrolyte replenishment because the working piece remains in the electrolyte for longer plating time compared to the multilayer case. Long plating times can promote the adsorption of hydrogen bubbles on the catalytic surface, thus blocking the growth of new nickel crystals and ultimately causing the formation of the defects visible on the surface of the sample. In the case of the r-monolayer coatings, the more vigorous stirring applied during the chemistry re-balance for faster homogenization of the electrolyte, might trigger H_2 bubbles desorption, giving rise to a defect free surface. Multilayered coatings are removed from the plating bath and rinsed several times between replenishment events, so there is a fresh surface free from defects associated to adsorbed species ready to be plated each time.

Multilayer and r-monolayer conditions showed thickness values of 22.7 ± 1.7 and 23.4 ± 0.3 μm and a phosphorous content of 2.0 ± 0.3 and 2.5 ± 0.2 wt. % respectively. In the case of the ur-monolayered coatings, the thickness was slightly lower showing a higher standard deviation standing at 19.2 ± 3.2 μm and having a phosphorous content of 3.0 ± 0.5 wt. %.

Chemically etched cross sections of the coatings were also evaluated as shown in Figure 1d-f and Figure 2d-f. Multilayered coatings showed the characteristic lamellar structure in each of the three stacks, which is typical of NiP coatings [23]. This lamellar structure is assumed to be caused by local fluctuations of the phosphorous content due to pH changes in the diffusion layer at the vicinity of the catalytic surface. Apart from the lamellar structure, two interfaces can be clearly distinguished as a result of the interruption of the electroless process. As depicted in Figure 1-d, the three different layers have similar thickness (about 7 μm each). After annealing, the lamellar structure becomes a bit ill-defined due to metallic matrix recrystallization (Figure 2-d). The interfaces resulting from the on-off electroless, though, remain more distinguishable. GDOES analyses clearly demonstrate the occurrence of these interfaces created throughout the coatings' thickness (estimated from sputtering time), as can be seen in Figure 3, in concordance with the phosphorous content profile measured by EDX and depicted in Table 1. Interestingly, no phosphorous diffusion occurred during annealing since the stepped profile remained the same as in the as-deposited state (Figure 3).

The cross-section of the NiP monolayered coatings produced from the un-rebalanced solution (ur-monolayer) was drastically different from the multilayered coatings, evolving from a lamellar to a columnar structure as the deposit builds up (Figure 1-e). This behaviour is assumed to be associated with the unbalanced chemistry of non-replenished electrolytes at long plating times. The occurrence of defects, some of them being "V" shaped, and promoted by substrate's roughness, are also visible. Annealing of these coatings had a similar effect on coating's microstructure, blurring the original microstructure (Figure 2-e). No apparent changes in phosphorous distribution upon annealing can be gleaned from GDOES analysis (Figure 3).

Figure 1-f shows the cross-section microstructure of the as-deposited r-monolayer coating obtained from the balanced electrolyte. The characteristic lamellar structure is clearly visible as well as two pseudo-interfaces matching the replenishment events performed during

plating. Such interfaces are analogous to those observed in the multilayered coating and are similar to those reported by Vitry et al. [24]. The occurrence of these interfaces is thought to be associated with unbalanced solution chemistry during replenishment, which leads to a different grain growth until the equilibrium is reached again. Defects of the coatings related to substrate roughness were also clearly identified. Thus, flat areas of the coatings showed defect free regions whereas rough areas were more prone to promote defects. "V" shaped defects were also detected, which crossed the coating's thickness almost entirely, reaching the substrate in many cases, and indicating a decreased ability for an effective protection of the substrate. After annealing the lamellar structure was almost lost but the pseudo-interfaces originated from bath replenishment were still visible (Figure 2-f). Similar to the multilayered coatings, cracks associated to substrate roughness smoothed and could not be further straightforwardly identified. In terms of chemical composition, these coatings showed a similar trend as the multilayer coatings. The location of the interfaces can be gleaned from the profile and the overall phosphorus content is slightly higher. Again, the distribution of phosphorous inside the coating did not change upon annealing (Figure 3).

3.2. XRD analysis

Figure 4-a shows the diffractogram of the coatings obtained from the three different conditions. The deposits are all nanocrystalline as expected from the relatively low phosphorous content in the coatings [7]. Diffraction pattern analysis revealed that the peaks can be indexed to the face-centred cubic (fcc) phase of Ni. The strongest reflection observed at $2\theta=44.5^{o}$ in all diffractograms corresponds to the (111) plane. Besides, a weaker reflection at $2\theta=51.8^{o}$ matching the (220) plane and other characteristic less intense reflections of the fcc Ni phase are observed, in agreement with PDF 065-2865. Only as-deposited ur-monolayer coatings showed some slight differences in the (200) plane probably due to a different crystal growth resulted from unbalanced bath chemistry at long plating times. The crystallite size determined from the Scherrer's equation is around 5-6 nm for all coatings (Table 2).

Annealing of the deposits promote the re-crystallization of the nickel matrix as seen from the narrowing of the diffraction peaks (Figure 4-b). Again, the (111) reflection is by far the most intense. The relative intensity of the (200) plane is lowered for the ur-monolayered coating compared to the other two. The precipitation of the tetragonal (BCT) Ni_3P phase is detected in all cases. Cristal size analysis confirms the re-crystallization of the metallic matrix. As a result, the crystal size increased by almost 10 fold (44-51 nm) after annealing for all studied conditions except for the ur-monolayer coating, for which the crystal size is slightly lower. Yet, the crystal sizes remain in the nano regime.

3.3. Mechanical properties

Representative load-unload displacement curves for the different coatings are shown in Figure 5, both in the as-prepared and annealed states. Table 3 lists the corresponding hardness (H) and reduced Young's modulus (E_r) values. ~~A slight reduction in H and E_r along the coatings' thickness (i.e., when moving toward the surface/air side) is observed in the as-deposited condition regardless of the plating approach undertaken. Considering that the indentations were performed at ~3.5 (L1), ~11 (L2) and ~17 (L3) µm from the substrate, slight microstructural changes as a function of depth rather than variations in the P content (Figure 3) might account for the variations in H in each sample. Recall that the amount of P changes by less than 1 wt.% within the whole indented area.~~ Results indicate that ~~The~~ E_r and H values are very similar among the three samples, in agreement with the similar crystal structure and crystallite size measured from XRD diffraction ~~despite the differences revealed by the cross-section FESEM images.~~ These results also indicate~~s~~ that the mechanical properties are not sensitive to the change from lamellar to columnar growth revealed by the cross-section FESEM images ~~microstructure~~ in the coatings fabricated using the different synthetic approaches~~, likely due to the very local nature of the indentations performed.~~ Typically, low P amounts are added to Ni coatings to increase its hardness [25]. The enhanced mechanical performance has been attributed to the supersaturated solid solution strengthening

and to grain size refinement caused by P addition following the Hall-Petch relationship [25]. Upon annealing, an increase in H and E_r can be observed for the three different coatings. This increase can be mainly attributed to the precipitation of hard Ni_3P intermetallic phase (detected by XRD, Figure 4-b) leading to precipitation hardening. Commonly, formation of Ni_3P phase in heat-treated Ni-P coatings has been reported to effectively increase its hardness [15,[25]. The monolayered coating prepared from the unadjusted solution shows, on average, a slightly higher H. Note that hardness values in excess of 10 GPa are obtained after annealing, which is comparable to the hardness of electrodeposited chromium [26] and the recently published electrodeposited Fe-25at%W [27].

3.4. Corrosion resistance

Table 4 summarizes the electrochemical corrosion parameters obtained for the as-deposited and annealed coatings in a chloride-containing electrolyte. As observed in the table, the corrosion potential (E_{corr}) was very similar for all the as-deposited electroless nickel surfaces (-300 ± 25 mV vs. Ag/AgCl), in agreement with their analogous chemical composition. Among the as-deposited coatings, multilayered coatings showed a slightly lower corrosion current density although no significant differences on polarization resistance neither on the Tafel slopes were observed.

Potentiodynamic behaviour (Figure 6a) of all as-deposited nickel coatings present similar characteristics. The anodic potentiodynamic curves show two regions: in the first region from the OCP to ca. -150 mV vs Ag/AgCl, the current density shows a pseudo-passive corrosion mechanism with an anodic Tafel slope of about 80±5 mV dec^{-1}. In the second region, at potentials more positive than -200 mV vs Ag/AgCl, the current increases rapidly with the applied potential, indicating a breakdown of the passivity and the on-set of localized corrosion. No significant differences were observed among the cathodic branches of the polarization curves.

To further understand the corrosion behaviour of the nickel coatings, both surface and cross-section observations were carried out by FESEM after the potentiodynamic polarizations. In all cases, surface micrographs of as-deposited coatings (Figure 7 a-c) indicate that the corroded areas show intergranular corrosion located at the boundaries of the nodules. A closer examination of the ur-monolayer coating reveals the presence of some debris on the surface of the coatings, not present on the multilayered and r-monolayered coatings. Observation of the surface at higher magnifications (Figure 8) indicated that the debris corresponded to NiP fibres that form the columnar microstructure, detached during the electrochemical polarization from the matrix by selective dissolution attack at the fibre boundaries. As a result, a fray-like effect along the thickness up to 5 µm depth into the coating`s was observed. This feature must be directly linked to the columnar microstructure shown by the ur-monolayer coating. The Cl^- anion preferentially attacks the coating through the column boundaries, creating multiple attack paths towards the substrate. This phenomenon, not observed on the multi-layered and r-monolayered coatings, points to differences in the coating's performance as a function of the plating mode that were not evident from the potentiodynamic tests.

Cross-section evaluation of chemically etched corroded samples was helpful to understand the corrosion mechanisms operating in the different as-deposited electroless nickel coatings. As shown in Figure 9-a, the multilayered coating did not fully protect the substrate, but the micrograph shows that the interfaces created in the synthetic approach hinder the progress of the corrosion attack; thus, some of the cracks promoted by the corrosive media become effectively blocked and do not reach the substrate. In the case of the ur-monolayer coatings, the corrosive attack consists of a microselective dissolution at the fibre boundaries (Figure 9b). Finally, in the r-monolayer coatings, the corrosive attack proceeds along the intrinsic defectivity of the coatings. Thus, when the Cl^- anions reach a defect, the attack

progresses directly to the substrate, indicating that the pseudo-observed-interfaces of the r-monolayer do not efficiently block the defect advancement.

Annealing brings about an enhancement of the corrosion resistance regardless the followed plating approach (Table 4). Thus, after annealing there is a shift of about 150 mV toward more positive values of the E_{corr}, an increase of the polarization resistances and anodic Tafel slopes and a decrease of corrosion current densities, indicating changes in composition, better passivity and a decreased corrosion susceptibility. A possible explanation for the generalized improvement of the corrosion resistance upon annealing for all coatings relies on the differences in crystallinity before and after thermal annealing. As-deposited coatings are nanocrystalline, with crystallite sizes in the range of 4.7-5.6 nm, and therefore characterized by a great amount of grain boundaries. These grain boundaries trigger the development of microcells which can pave the way for the advancement of the corrosive attack[29]. Annealing of the coatings brings about an increase of almost ten-fold in the crystallite size which diminishes the density of grain boundaries and, in turn, improves the corrosion resistance. This reduction in the grain boundaries due to grain coarsening dominates over the effect imparted by Ni_3P phase precipitation, which could act in parallel as active sites for corrosion attack [30].

Corrosion performance of annealed coatings was found to be notably different from that of the as-deposited coatings (Figure 9). Surface observation revealed a change in the corrosion mechanism from localized intergranular corrosion initiated at the nodule boundaries for the as-deposited coatings to localized pitting corrosion when annealed coatings were tested. Pitting corrosion phenomena was exacerbated in the monolayered coatings (Figure 7 d-f). Cross-sections analysis of the samples after corrosion tests, also indicated additional differences among the coatings. Annealed multilayered coatings were still protecting the substrate and no sign of red corrosion was observed. The multilayered coating dissolves layer by layer underlining the layer-type morphology of the coatings. It is hypothesized that once

the corrosive attack proceeds through the first layer, it stops at the interface where the corrosion products spread laterally, leading to exfoliation of the outermost layer and causing the exposure of the layer beneath to the corrosive media (Figure 9-d). A similar mechanism has been previously proposed for NiP electrodeposited multilayers[31]. Annealing of the ur-monolayered coatings have a similar behaviour compared to the multilayered case. Figure 9-e show a more homogeneous coating in which the lamellar structure is imperceptible due to metallic matrix recrystallization. Yet, some defects are still visible across the coating's surface which, when exposed to the corrosive media, facilitates that chloride anions progress through these defects ultimately reaching the substrate and leading to a complete detachment of V-shaped fragments of the coating. On the other hand, Figure 9-f shows the cross-section of an annealed r-monolayer coating after polarization. The image shows that the coating gets progressively dissolved by the corrosive media until it finds a weak point which allows the attack of the substrate by pit formation.

These results highlight the importance of chemical solution maintenance at long plating times as well as the effect of the plating approach used for the production of high-quality electroless coatings for demanding applications.

4. Conclusions

Electroless nickel multilayered and monolayered coatings were produced from a proprietary low phosphorous nickel electrolyte. As-deposited coatings were nano-crystalline, dense and homogeneous in all the cases. At higher magnification, though, ur-monolayered coatings, showed some defects like small pores. The multilayered coatings were characterized by well-defined interfaces stemming from process interruption, which effectively prevent crack propagation along the coating thickness, thereby offering better protection ability compared with the monolayered coatings. r-monolayered coatings showed interfaces analogous to the multilayer case, matching the replenishment events performed during plating. Such interfaces do not completely protect the surface and defects are able to traverse

the coating´s thickness, reaching more easily the substrate without getting blocked at the interfacial region. As result of the unbalanced chemistry of the electrolyte at long plating times, the ~~microstructure~~ growth of the ur-monolayered coatings evolved from lamellar to columnar type. Annealing of the coatings promotes the recrystallization of the metallic matrix, thereby increasing the crystallite size by tenfold and giving rise to coatings with fewer defects or weak points. Interfaces were still visible for both multilayer and r-monolayered coatings but the fine lamellar microstructure was almost lost.

Nanoindentation experiments performed on the as-deposited coatings' cross-sections revealed that hardness and reduced Young's modulus were very similar despite the differences observed by FESEM, in agreement with the similar crystalline structure revealed by XRD analysis. ~~This indicates that composition rather than microstructural variations along the coating thickness is playing a dominant role.~~ Upon annealing, both parameters increased, presumably due to precipitation of Ni_3P.

Corrosion analysis of as-deposited coatings indicated intergranular corrosion located at the surface nodules boundaries. Microstructural characterization revealed significant changes among the coatings. Thus, while the interfaces of the multilayered coatings delay the progress of the corrosive attack by blocking the advance of the defects produced by the corrosive media, in the monolayered coatings the corrosion progress through the coating reaching the substrate, aggravated in the case of ur-monolayered coatings. After annealing, corrosion performance of the NiP coatings improved as a result of reduced grain boundary due to grain coarsening. Moreover, a change from intergranular to pitting corrosion was observed. Cross-section evaluation indicated that the interfaces of the annealed multilayered coatings successfully prevent the progress of the corrosive attack, unlike monolayered coatings. According to the results, annealed electroless nickel multilayers allows obtaining coatings with enhanced corrosion resistance, compared to monolayered coatings, while maintaining their mechanical properties.

Acknowledgments

The authors would like to acknowledge the EU funded COST Action MP-1407 "e-minds" for their networking support. One of the authors also acknowledge COST Action MP-1407 "e-minds" for their financial support for carrying out a STSM at Udine University which greatly contributes to this article. This work was also partially supported by the Spanish Government (MAT2017-86357-C3-1-R, MAT2017-86357-C3-2-R projects), by the Departamento de Desarrollo Económico y Competitividad of the Basque government (ELKARTEK, KK-2017/00096, KK-2018/00108) and Generalitat de Catalunya (2017-SGR-292). AS acknowledges the PhD programme in Materials Science from Universitat Autònoma de Barcelona in which he is enrolled.

References

[1] A. Brenner, G.E. Riddell, Nickel plating on steel by chemical reduction, J. Res. Natl. Bur. Stand. (1934). 37 (1946) 31–34. doi:10.6028/jres.037.019.

[2] E.J. O'Sullivan, Fundamental and practical aspects of the electroless deposition reaction, in: D.M.K. Richard C. Alkire (Ed.), Adv. Electrochem. Sci. Eng., Wiley-VCH, 2001: pp. 225–273.

[3] D. Ahmadkhaniha, F. Eriksson, P. Leisner, C. Zanella, Effect of SiC particle size and heat-treatment on microhardness and corrosion resistance of NiP electrodeposited coatings, J. Alloys Compd. 769 (2018) 1080–1087. doi:10.1016/j.jallcom.2018.08.013.

[4] N. Imaz, J.A. Díez, M. Ostra, M. Sarret, E. García-Lecina, Advanced Ni–W coatings obtained by the combination of pulse plating and chemometric techniques, Trans. IMF. 92 (2014) 305–315. doi:10.1179/0020296714Z.000000000214.

[5] N. Imaz, M. Ostra, M. Vidal, J.A. Díez, M. Sarret, E. García-Lecina, Corrosion behaviour of chromium coatings obtained by direct and reverse pulse plating electrodeposition in NaCl aqueous solution, Corros. Sci. 78 (2014) 251–259. doi:10.1016/j.corsci.2013.10.005.

[6] J.N. Balaraju, N. Raman, N.T. Manikandanath, Nanocrystalline electroless nickel poly-alloy deposition: incorporation of W and Mo, Trans. IMF. 92 (2014) 169–176. doi:10.1179/0020296713Z.000000000123.

[7] G.G.O. Mallory, J.B. Hajdu, Electroless Plating: Fundamentals And Applications, 1990. doi:10.1155/APEC.3.103.

[8] W. Riedel, Electroless Nickel Plating, ASM International, 1991. https://books.google.es/books?id=XX9xQgAACAAJ.

[9] J. Sudagar, J. Lian, W. Sha, Electroless nickel, alloy, composite and nano coatings - A critical review, J. Alloys Compd. 571 (2013) 183–204. doi:10.1016/j.jallcom.2013.03.107.

[10] G.G. Gawrilov, Chemical (electroless) nickel plating, Portcullis Press Ltd., 1979.

[11] D. Baudrand, B. Durkin, Automotive Applications of Electroless Nickel, Met. Finish. 96 (1998) 20–23. doi:10.1016/S0026-0576(98)80080-9.

[12] F.B. Mainier, M.P.C. Fonseca, S.S.M. Tavares, J.M. Pardal, Quality of electroless Ni-P (nickel-phosphorus) coatings applied in oil production equipment with salinity, J. Mater. Sci. Chem. Eng. 1 (2013) 1–8. doi:10.4236/msce.2013.16001.

[13] G. Cui, S. Liu, K. Wang, Q. Li, G. Wu, Discovering p-doped mechanism in non-magnetic Ni–P films for HDD substrate: a combined experimental and theoretical study, RSC Adv. 4 (2014) 14663. doi:10.1039/c3ra47217e.

[14] M.C.L. de Oliveira, O.V. Correa, B. Ett, I.J. Sayeg, N.B. de Lima, R.A. Antunes, Influence of the Tungsten Content on Surface Properties of Electroless Ni-W-P Coatings, Mater. Res. 21 (2017) 1–13. doi:10.1590/1980-5373-MR-2017-0567 ©.

[15] M. Czagány, P. Baumli, G. Kaptay, The influence of the phosphorous content and heat treatment on the nano-micro-structure, thickness and micro-hardness of electroless Ni-P coatings on steel, Appl. Surf. Sci. 423 (2017) 160–169. doi:10.1016/j.apsusc.2017.06.168.

[16] P. De Lima-neto, A.N. Correia, R.A.C. Santana, R.P. Colares, E.B. Barros, P.N.S. Casciano, G.L. Vaz, Morphological , structural , microhardness and electrochemical characterisations of electrodeposited Cr and Ni – W coatings, Electrochim. Acta. 55 (2010) 2078–2086. doi:10.1016/j.electacta.2009.11.037.

[17] T.S.N. Sankara Narayanan, I. Baskaran, K. Krishnaveni, S. Parthiban, Deposition of electroless Ni-P graded coatings and evaluation of their corrosion resistance, Surf. Coatings Technol. 200 (2006) 3438–3445. doi:10.1016/j.surfcoat.2004.10.014.

[18] S.R. Anvari, S.M. Monirvaghefi, M.H. Enayati, Novel Investigation on Nanostructured Multilayer and Functionally Graded Ni-P Electroless Coatings on Stainless Steel, J. Mater. Eng. Perform. 24 (2015) 2373–2381. doi:10.1007/s11665-015-1533-y.

[19] C. Gu, J. Lian, G. Li, L. Niu, Z. Jiang, High corrosion-resistant Ni-P/Ni/Ni-P multilayer coatings on steel, Surf. Coatings Technol. 197 (2005) 61–67. doi:10.1016/j.surfcoat.2004.11.004.

[20] V. Vitry, L. Bonin, Formation and characterization of multilayers borohydride and hypophosphite reduced electroless nickel deposits, Electrochim. Acta. 243 (2017) 7–17. doi:10.1016/j.electacta.2017.04.152.

[21] B. Zhang, Amorphous and Nano Alloys Electroless Depositions, 2016. http://www.sciencedirect.com/science/article/pii/B9780128026854000042.

[22] M.A.L.G. Stern, Electrochemical Polarization, J. Electrochem. Soc. 104 (1957) 559. doi:10.1149/1.2428653.

[23] C.C. Nee, R. Weil, The banded structure of Ni-P electrodeposits, Surf. Technol. 25 (1985) 7–15. doi:10.1016/0376-4583(85)90043-3.

[24] V. Vitry, A.F. Kanta, F. Delaunois, Evolution of reactive concentration during borohydride-reduced electroless nickel-boron plating and design of a replenishment procedure, Ind. Eng. Chem. Res. 51 (2012) 9227–9234. doi:10.1021/ie202687y.

[25] H.C. Huang, S.T. Chung, S.J. Pan, W.T. Tsai, C.S. Lin, Microstructure evolution and hardening mechanisms of Ni-P electrodeposits, Surf. Coatings Technol. 205 (2010) 2097–2103. doi:10.1016/j.surfcoat.2010.08.115.

[26] D. Wu, J. Zhang, J.C. Huang, H. Bei, T.G. Nieh, Grain-boundary strengthening in nanocrystalline chromium and the Hall-Petch coefficient of body-centered cubic metals, Scr. Mater. 68 (2013) 118–121. doi:10.1016/j.scriptamat.2012.09.025.

[27] A. Nicolenco, N. Tsyntsaru, J. Fornell, E. Pellicer, J. Reklaitis, D. Baltrunas, H. Cesiulis, J. Sort, Mapping of magnetic and mechanical properties of Fe-W alloys electrodeposited from Fe(III)-based glycolate-citrate bath, Mater. Des. 139 (2018) 429–438. doi:10.1016/j.matdes.2017.11.011.

[28] J.N. Balaraju, V.E. Selvi, V.K.W. Grips, K.S. Rajam, Electrochemical studies on electroless ternary and quaternary Ni-P based alloys, Electrochim. Acta. 52 (2006)

1064–1074. doi:10.1016/j.electacta.2006.07.001.

[29] Y. Gao, Z.J. Zheng, M. Zhu, C.P. Luo, Corrosion resistance of electrolessly deposited Ni-P and Ni-W-P alloys with various structures, Mater. Sci. Eng. A. 381 (2004) 98–103. doi:10.1016/j.msea.2004.04.077.

[30] T. Rabizadeh, S.R. Allahkaram, A. Zarebidaki, An investigation on effects of heat treatment on corrosion properties of Ni-P electroless nano-coatings, Mater. Des. 31 (2010) 3174–3179. doi:10.1016/j.matdes.2010.02.027.

[31] L. Elias, K.U. Bhat, A.C. Hegde, Development of nanolaminated multilayer Ni–P alloy coatings for better corrosion protection, RSC Adv. 6 (2016) 34005–34013. doi:10.1039/C6RA01547F.

Table 1. Coating characterization (thickness, P content and average surface roughness) for the different electroless nickel coatings in the as-deposited state.

Condition	Thickness (µm)	P content (%wt.)	Surface Roughness (S_a) (µm)
Multilayer	22.7 ± 1.7	2.0 ± 0.3	1.8
r-monolayer	23.4 ± 0.3	2.5 ± 0.2	1.7
ur-monolayer	19.2 ± 3.2	3.0 ± 0.5	1.6

Table 2. Crystallite size obtained using the Scherrer's equation on the (111) peak width

	Crystallite size (nm)	
	As-deposited	**Annealed**
Multilayer	5.6	51.1
r-monolayer	4.7	44.4
ur-monolayer	4.9	32.4

Table 3. Hardness and Young's modulues values of the electroless NiP coatings determined by nanoindentation

CONDITION		As-deposited		Annealed	
		H (GPa)	E_r (GPa)	H (GPa)	E_r (GPa)
Multilayer	**L_1**	9.48±0.17	174.5±2.2	10.42±0.21	214.5±6.4
	L_2	9.40±0.15	166.4±2.2	10.36±0.17	213.3±4.9
	L_3	9.15±0.32	140.3±8.6	10.15±0.23	197.0±6.4
r-monolayer	**L_1**	9.80±0.15	171.6±2.3	10.98±0.39	220.6±4.8
	L_2	9.52±0.23	168.2±2.6	11.11±0.25	218.7±3.8
	L_3	9.47±0.09	156.8±3.2	10.40±0.27	201.5±8.3
ur-monolayer	**L_1**	9.57±0.17	168.5±2.3	11.15±0.23	215.3±3.8
	L_2	9.54±0.12	166.6±3.0	11.34±0.17	210.9±4.0
	L_3	9.44±0.15	151.7±5.2	10.68±0.08	188.6±9.7

Table 4. Electrochemical parameters obtained after electrochemical corrosion tests.

CONDITION	$-E_{corr}$ (mV vs. Ag/AgCl)	R_p (kΩ cm^2)	b_a (mV dec^{-1})	$-b_c$ (mV dec^{-1})	j_{corr} (μA cm^{-2})
As-deposited coatings					
Multilayer	282±5	29±1	76±5	92±1	0.63±0.05
r-monolayer	322±8	23±2	84±9	96±2	0.85±0.11
ur-monolayer	332±11	16±1	78±9	90±1	1.14±0.15
Annealed coatings					
Multilayer	154±9	41±4	109±3	65±3	0.43±0.09
r-monolayer	161±15	31±7	124±9	68±4	0.61±0.15
ur-monolayer	186±13	25±9	129±6	44±4	0.57±0.19

Figure captions

Figure 1. Surface morphology and corresponding etched cross-sections of as-deposited electroless NiP coatings, respectively, for (a, d) multilayered, (b, e) ur-monolayered and (c, f) r-monolayered cases.

Figure 2. Surface morphology and related chemically etched cross-section of annealed electroless NiP coatings: (a,d) multi-layered, (b, e) ur-monolayered and (c, f) r-monolayered cases.

Figure 3. Compositional profiles obtained by GDOES analysis for a) as-deposited and b) annealed NiP coatings where a) multilayer, b) ur-monolayer and c) r-monolayer.

Figure 4. XRD patterns of a) as-deposited and b) annealed NiP coatings where a) multilayer, b) ur-monolayer and c) r-monolayer.

Figure 5. Load vs depth curves obtained from nanoindentation tests for as-deposited and annealed NiP coatings where a) multilayer b) ur-monolayer and c) r-monolayer

Figure 6. Polarization curves of a) as-deposited and b) annealed NiP electroless coatings where a) multilayer, b) ur-monolayer and c) r-monolayer.

Figure 7. Surface morphology of (a-c) as-deposited and (d-f) annealed electroless NiP coatings after polarization studies where (a, d) multilayered, (b, e) ur-monolayered and (c, f) r-monolayered coatings.

Figure 8. Zoomed details of surface morphology of as-deposited ur-monolayered NiP coatings after polarization studies.

Figure 9. Chemically etched cross-section analysis after polarization tests of as-deposited (a-c) and annealed (d-f) electroless NiP coatings where (a, d) multilayered, (b, e) ur-monolayered and (c, f) r-monolayered coatings.

Highlights

- Monolayered and multilayered NiP electroless coatings were produced from a proprietary low phosphorous nickel electrolyte.
- The multilayered coatings were characterized by well-defined interfaces due to process interruption.
- Interfaces of multi-layered coatings block crack propagation and corrosion progress.
- Multilayered coatings exhibit enhanced corrosion resistance in comparison to monolayered coatings.

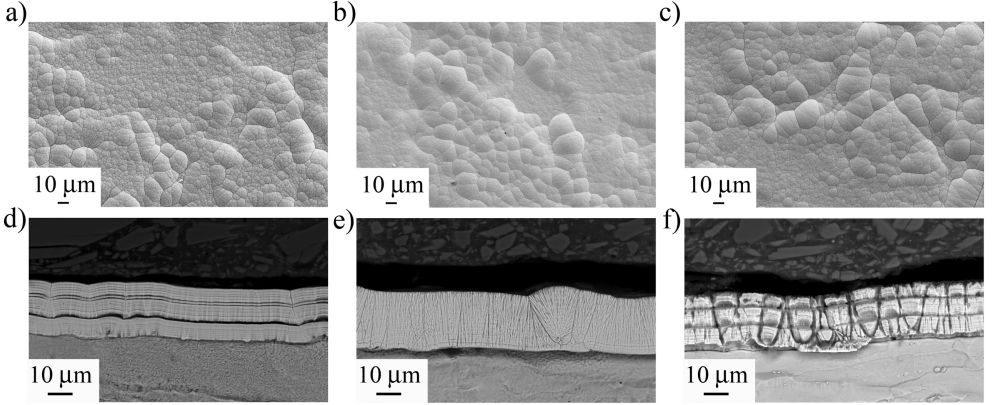

Figure 1

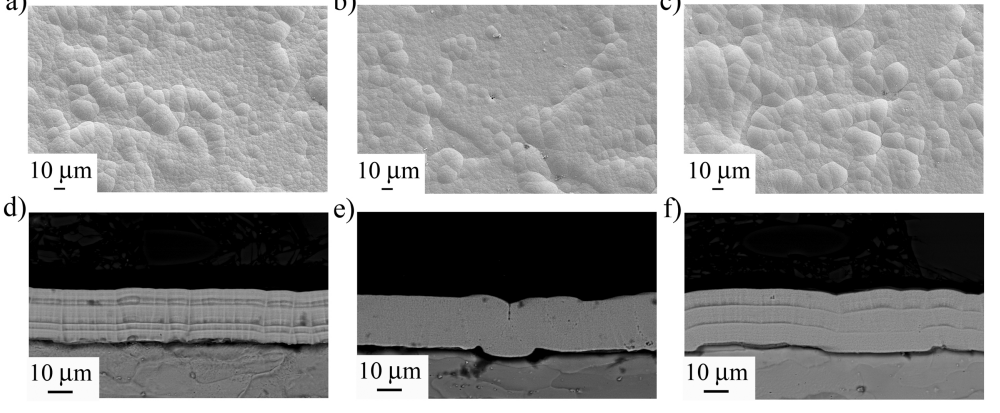

Figure 2

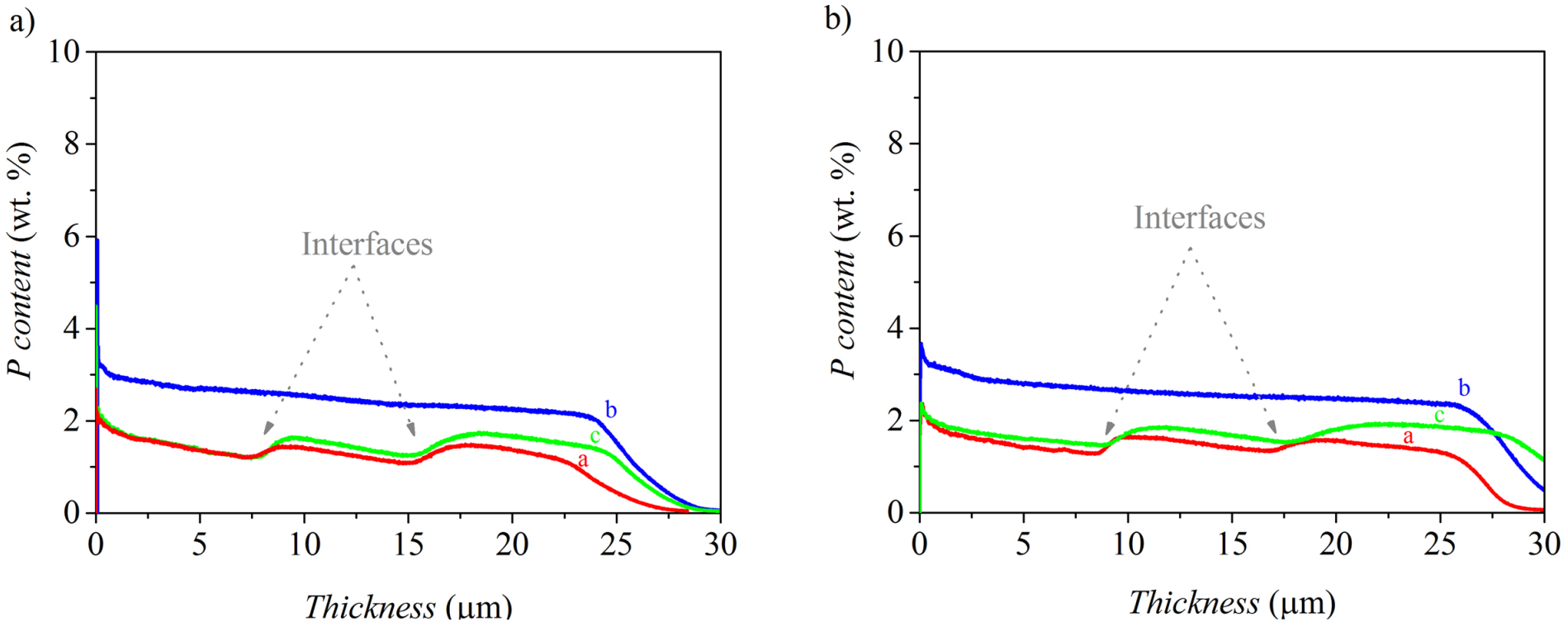
a)
b)
P content (wt. %)
Thickness (μm)
Interfaces
a
b
c
0
2
4
6
8
10
0
5
10
15
20
25
30

Figure 3

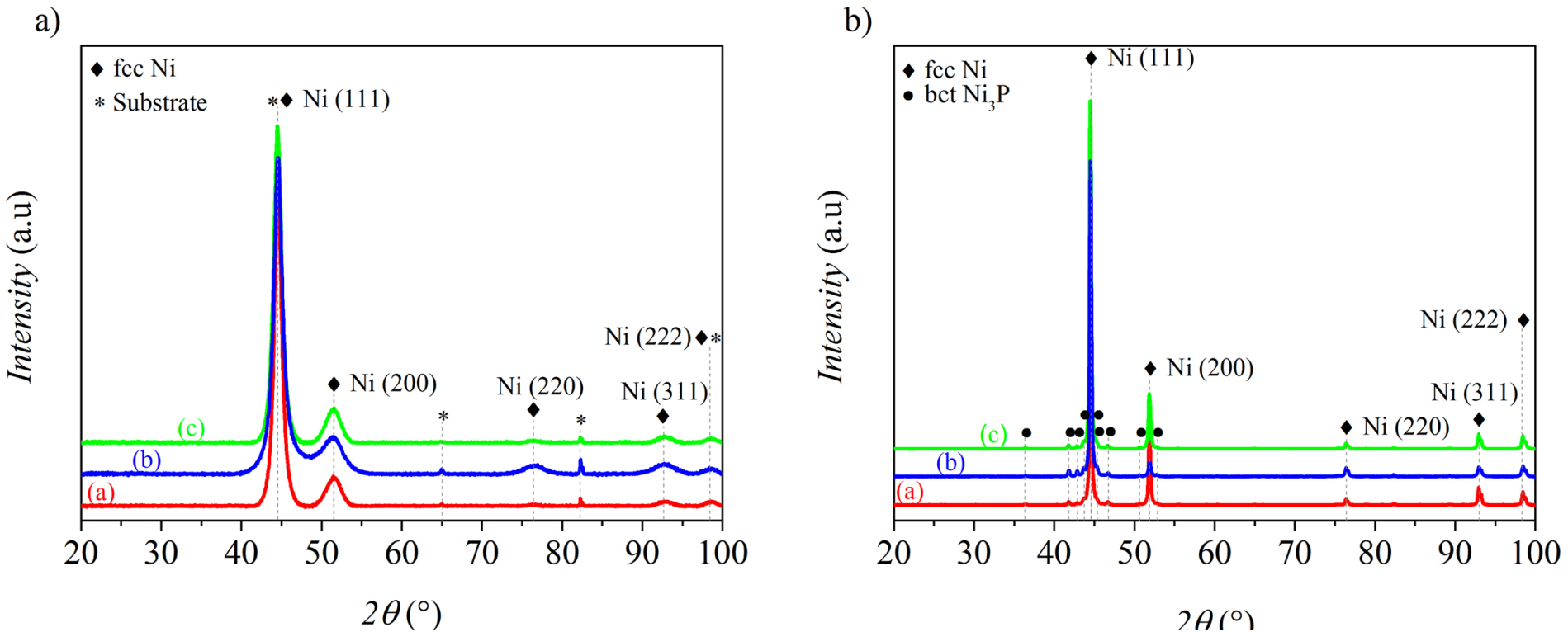
a)
fcc Ni
Substrate
Ni (111)
Ni (200)
Ni (220)
Ni (311)
Ni (222)
(c)
(b)
(a)
Intensity (a.u)
2θ (°)
b)
fcc Ni
bct Ni3P
Ni (111)
Ni (200)
Ni (220)
Ni (311)
Ni (222)
(c)
(b)
(a)
Intensity (a.u)
2θ (°)

Figure 4

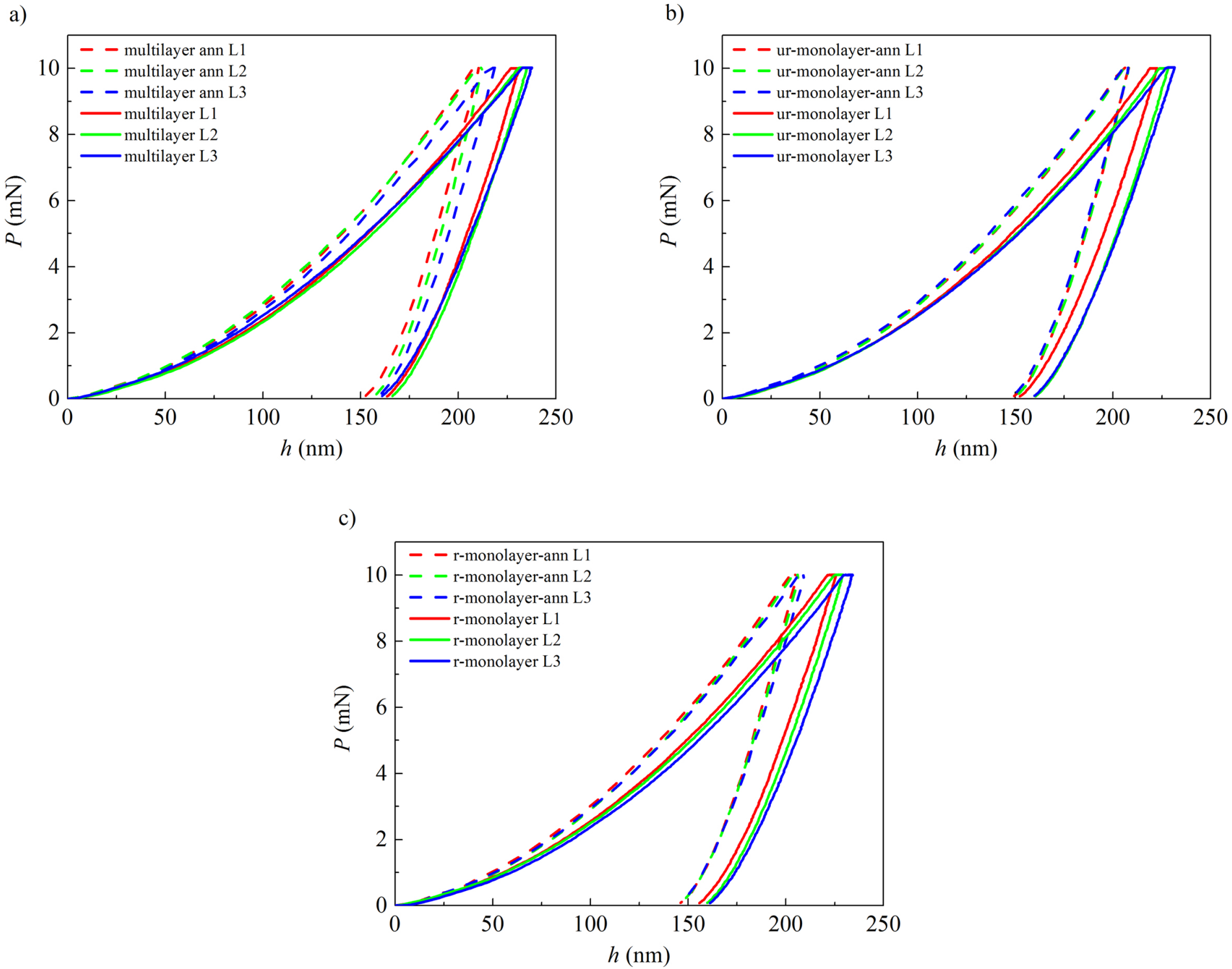
a)
multilayer ann L1
multilayer ann L2
multilayer ann L3
multilayer L1
multilayer L2
multilayer L3
P (mN)
h (nm)
b)
ur-monolayer-ann L1
ur-monolayer-ann L2
ur-monolayer-ann L3
ur-monolayer L1
ur-monolayer L2
ur-monolayer L3
P (mN)
h (nm)
c)
r-monolayer-ann L1
r-monolayer-ann L2
r-monolayer-ann L3
r-monolayer L1
r-monolayer L2
r-monolayer L3
P (mN)
h (nm)

Figure 5

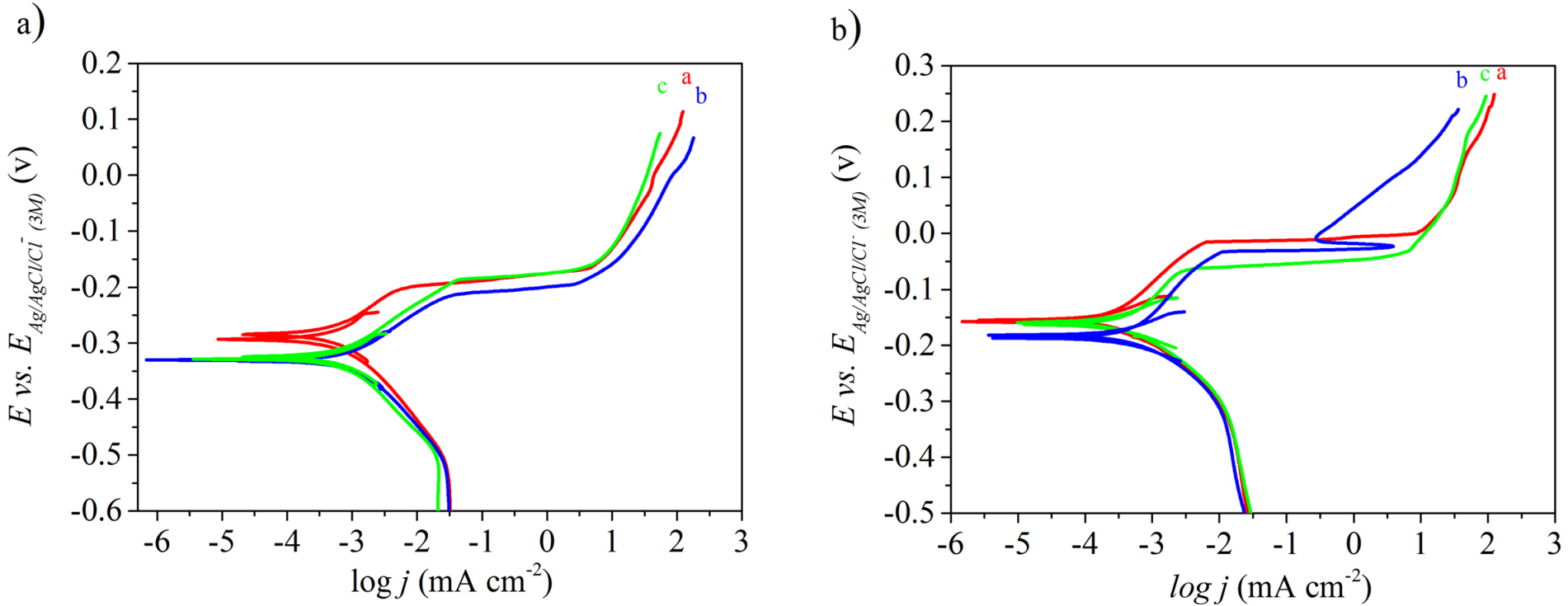

Figure 6

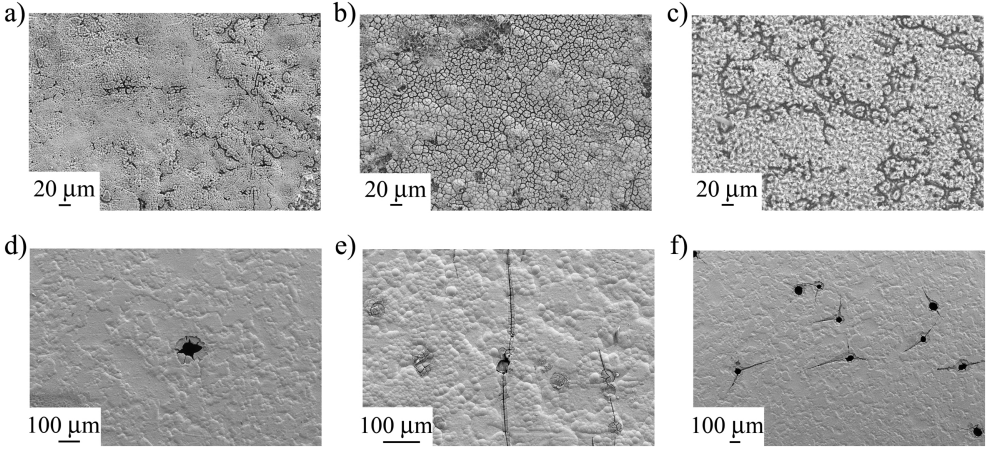

Figure 7

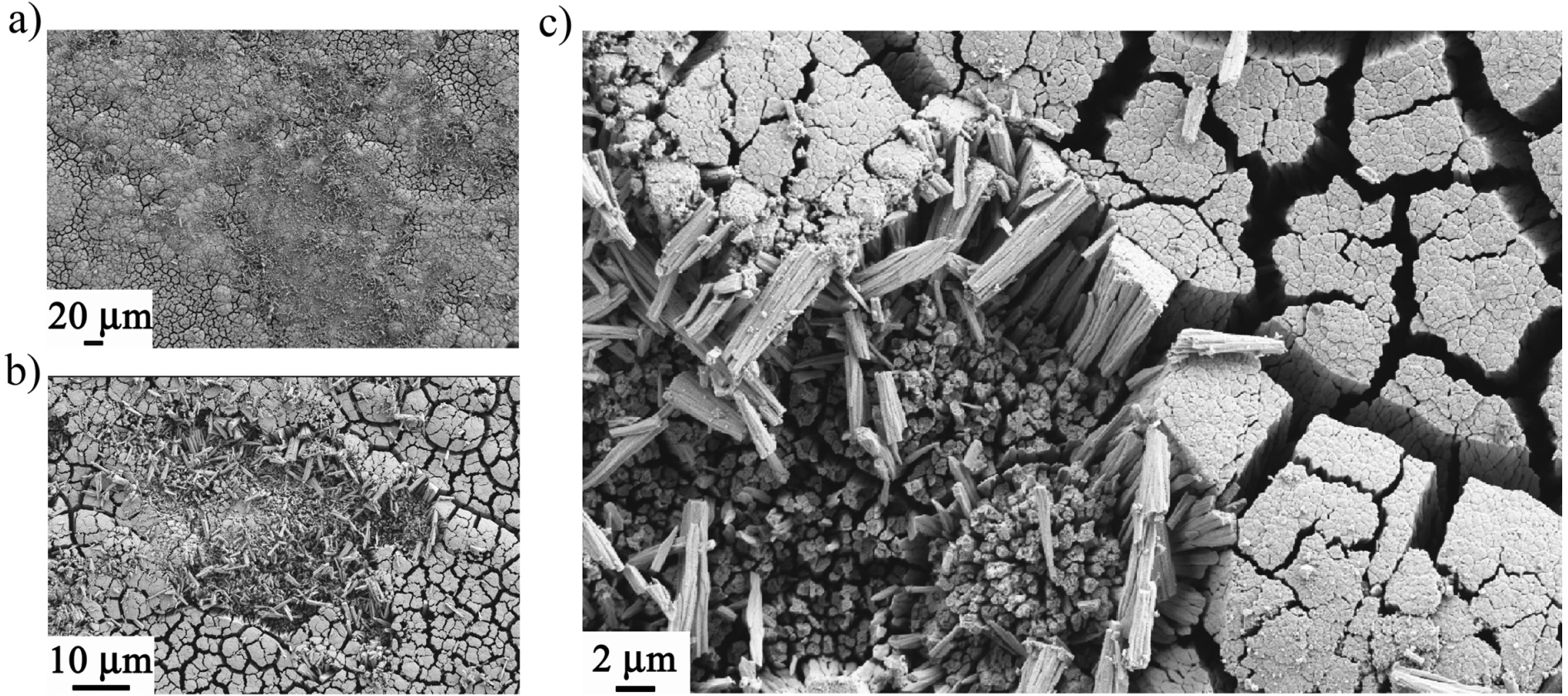

Figure 8

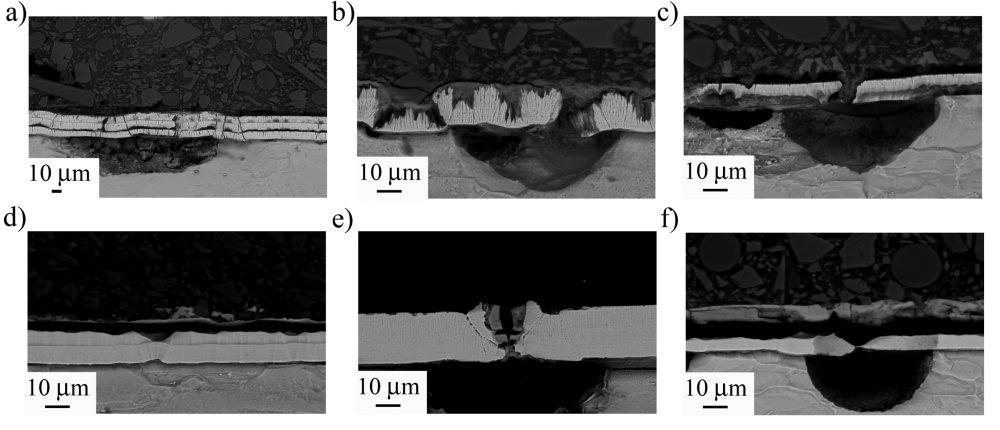

Figure 9